THE JOURNAL OF PHYSICAL CHEMISTRY B

pubs.acs.org/JPCB Article

Effect of Loop Defects on the High Strain Rate Behavior of PEGDA Hydrogels: A Molecular Dynamics Study

Ke Luo, Charity Wangari, Ghatu Subhash, and Douglas E. Spearot*

Cite This: J. Phys. Chem. B 2020, 124, 2029–2039 Read Online

ACCESS | Metrics & More | Article Recommendations

ABSTRACT: The high strain rate behavior of nonideal poly(ethylene glycol) diacrylate hydrogels under uniaxial tension and transient-state shear deformations is investigated using molecular dynamics (MD) simulations. This work specifically focuses on the influence of first-order loop defects, including their effect on topological evolutions. Two approaches are proposed to systematically introduce first-order loops, allowing separate and controllable investigations of effective cross-link functionality and cross-link density. MD simulations confirm that first-order loop defects are elastically inactive, but the topological disruptions caused by the presence of loop defects influence mechanical behavior. For decreasing effective cross-link functionality but constant cross-link density, a weaker tensile stress−strain response and decreasing shear-thickening behavior are observed. This is due to nonaffine translation of cross-link junction positions during deformation. Hydrogels with lower cross-link density but constant effective functionality show a stronger stress−strain response and an earlier transition between entropic and enthalpic deformation regimes. This behavior is correlated to changes in mesh size caused by the introduction of loops within an elastically active network. However, the resulting range of cross-link densities is not sufficient to cause measurable changes in shear-thickening behavior. To conclude, reductions in effective cross-link functionality are more important to high strain rate behavior than reductions in cross-link density.

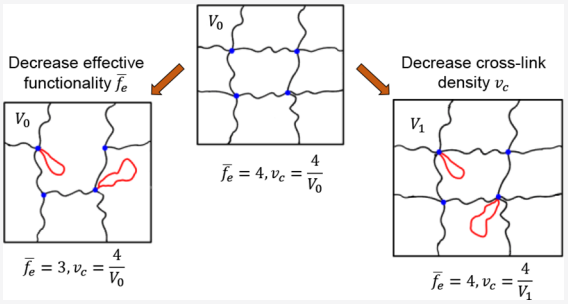

1. INTRODUCTION

Hydrogels are soft materials that are employed in a range of applications because of their stress-tolerant cross-linked polymer network and ability to retain water.[1−3] For example, biological scaffolds made of hydrogels can maintain a desired volume and structure for drug delivery and postoperative wound adhesion.[4] Tissue surrogates made of hydrogels can be fabricated to mimic the mechanical properties of human organs.[5] These applications require adequate understanding of hydrogel behavior under various deformation modes and conditions.

Current understanding of the mechanical properties of hydrogels is built on classical rubber elasticity theory with additional refinements (e.g., affine and phantom network theory), where the role of topology is considered via properties such as cross-link functionality and cross-link density.[6,7] However, the affine and phantom network theories predict elastic properties of hydrogels that deviate from experimental results.[8,9] This deviation can be attributed to the existence of structural imperfections in real hydrogels that are different from the ideal structure assumed in classical network theories.[10] These structural imperfections are recognized as defects.

Experimental evidence has indicated that defects exist at various length scales in hydrogel samples.[11] At the scale of the individual polymer chains, defects include dangling chains, unreacted chains, chain entanglements, and loops of different orders. At larger length scales, defects predominantly consist of spatial inhomogeneity of cross-link junctions. During hydrogel synthesis, the number of defects can be minimized via stoichiometric and kinetic control of the cross-linking reaction.[12] However, the formation of loops is inevitable due to the intrinsic intramolecular reactions between finite chain length polymers.[13] Therefore, understanding the influence of loop defects is essential to develop more accurate constitutive models for the mechanical response of hydrogels.

The role of loop defects in the mechanical properties of cross-linked polymers has been discussed in the literature for decades, where the main focus has been to modify the network elasticity equations to discard loops and only account for elastically active chains and cross-link junctions.[14−17] Early approaches to modify the equations of network elasticity were empirically based on experimental results of tensile or compressive deformation, where the exact number of loop defects was not known. With new techniques, such as network disassembly spectrometry (NDS) and multiple-quantum

Received: December 8, 2019
Revised: February 7, 2020
Published: February 10, 2020

https://dx.doi.org/10.1021/acs.jpcb.9b11378
J. Phys. Chem. B 2020, 124, 2029−2039

nuclear magnetic resonance (MQ NMR), quantitative determination of loop defects in polymers is possible.[11] Therefore, modern elasticity theories predict the mechanical response of network polymers considering loop concentrations. One example is the realistic elastic network theory (RENT) developed by Zhong et al.,[18] where combined experimental and Monte Carlo (MC) simulation results were used to quantify the influence of loop defects on network elasticity. Additional modifications have been made to the RENT theory to consider the influence of higher order loop defects,[19] odd/even effects,[14] etc. Although significant advancement is achieved in quantifying the influence of loop defects on the mechanical response of polymers under quasi-static conditions, it is not yet known to what extent the existing theories are applicable in the high strain rate regime; this is particularly important for hydrogels, which are known to be strain rate sensitive.[20,21]

Experiments have been conducted and theories have been developed to characterize the high strain rate behaviors of hydrogels under different deformation modes.[22−27] For example, visco-hyperelastic constitutive models have been derived to describe the uniaxial compressive and tensile responses of hydrogels at strain rates lower than 10^4 s^{-1}.[5,28,29] Hydrodynamic theory was applied when hydrogels were subjected to shock loading conditions at strain rates above 10^5 s^{-1}.[30] A power-law model was employed to capture the non-Newtonian fluid behavior of hydrogels under high strain rate shear conditions.[31,32] Regardless of the deformation mode or conditions, hydrogels demonstrate strong strain rate dependence, where the elastic modulus, strength, and viscosity are found to increase with strain rate. However, none of the prior studies has focused on the role of loop defects in mechanical behavior. Indirect insights are implied by the authors' prior study that showed shear-thickening exponents were overestimated in atomistic simulations compared to experiments, since the atomistic simulations used an ideal (defect-free) network model of poly(ethylene glycol) diacrylate hydrogel.[33] This observation suggests that defects have non-negligible influence on the high strain rate properties of hydrogels. Therefore, the objective of this work is to delineate the effect of loop defects on the high strain rate behavior of hydrogels via a systematic investigation of effective cross-link functionality and cross-link density, which are both influenced by the presence of loops.

Molecular dynamics (MD) simulation, which provides nanoscale resolution of the network topology, is an effective tool to study network defects in hydrogels.[34,35] One approach is via an ideal network model, where cross-linked networks are constructed with six chain connections, periodically distributed in three coordinate directions.[36,37] Although this model provides good estimations of material properties,[38] the absence of defects likely limits its accuracy. Other MD studies have developed a "reactive" approach to create nonideal polymer networks.[39,40] This method involves dynamic creation of covalent junctions via a series of bond creation (if-then) criteria. However, with this approach, the user has limited control over the final network characteristics because of the stochastic nature of the cross-linking method, which may result in unrealistic network topologies due to substantial differences in the time scale at which cross-link bonds are created between MD simulation and experiment. As the key goal of the current study is to understand the correlation between topological features and high strain rate behavior, a controllable method for loop defect introduction is required. Therefore, a new approach for creating cross-linked hydrogel models with purposely introduced loop defects is presented. The advantage of the proposed approach includes the precise control of network topology, defect type, and defect density. Thus, systematic studies of the influence of defects on the high strain rate behavior of hydrogels are conducted at various loop concentrations.

Two deformation modes are considered to study the high strain rate behavior of hydrogels: uniaxial tension and transient-state shear. Uniaxial tension simulations provide a simple boundary condition to develop and validate characterization methods for quantifying correlations between topology and mechanical properties. These topological characterization methods can be adopted to study the shear-thickening behavior of hydrogels under transient-state shear deformation.

2. SIMULATION DETAILS

2.1. Materials and Force Fields. The hydrogel selected is composed of poly(ethylene glycol) diacrylate (PEGDA) chains with a degree of polymerization of 13, swollen by water molecules to 20 wt % PEGDA concentration. PEGDA polymers are modeled using OPLS united-atom potentials,[41] and water molecules are explicitly modeled using the TIP3P flexible potential.[42] Previous studies by the current authors using this force field combination showed good agreement in equilibrium density and mesh size between simulations and experiments for PEGDA hydrogels.[30,33] The cutoff distance is set to 10 Å, and a long-range Coulomb correction is applied with the particle-particle particle-mesh (PPPM) method. All simulations are performed using LAMMPS.[43]

2.2. Topological Variables in a Hydrogel Network. The topology of an ideal hydrogel network can be described by three variables: cross-link density (ν_c), average cross-link functionality ($\overline{f}$), and average mesh size (ξ). The cross-link density represents the number density of cross-link junctions per unit volume

$$\nu_c = \frac{N}{V} \tag{1}$$

where N is total number of cross-link junctions and V is the volume of hydrogel. The average cross-link functionality, which describes the average number of polymer chain ends connected to a junction, is given by

$$\overline{f} = \frac{1}{N}\sum_{i=1}^{N} f_i \tag{2}$$

where f_i is the number of chain ends connected to an individual cross-link junction. The average mesh size is the average distance between consecutively connected cross-link junctions. It serves a critical role in connecting network structure with the mechanical properties of hydrogels. In experiments, mesh size is estimated from the Flory−Rehner model with preswelling factors.[44] In MD simulation, the measurement of mesh size can be done directly based on the known network topology. The details of the mesh size measurement are presented in Section 2.5.

If a hydrogel network contains defects, the average cross-link functionality is no longer of primary importance; instead, the effective cross-link functionality ($\overline{f}_e$), which only accounts for elastically active connections, can be computed via

https://dx.doi.org/10.1021/acs.jpcb.9b11378
J. Phys. Chem. B 2020, 124, 2029−2039

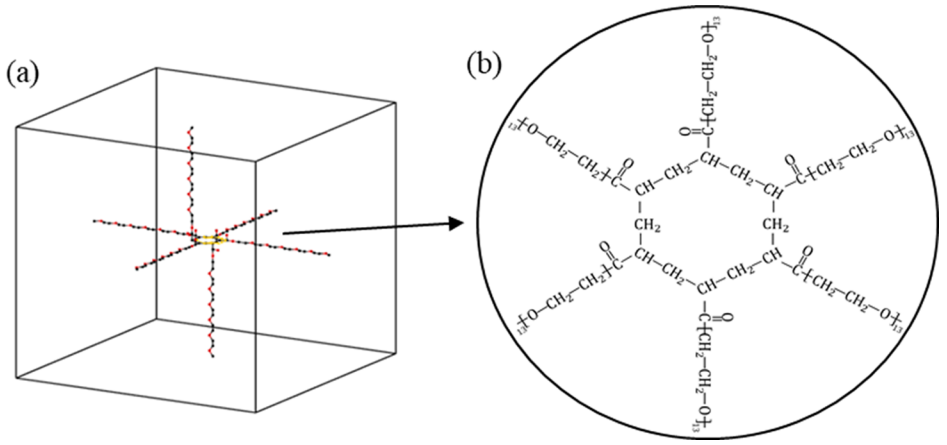

Figure 1. (a) Ideal PEGDA cross-link junction in MD simulation. Black represents the united-atom style CH_2 atoms, red represents O atoms, and yellow represents cross-link junctions. (b) Enhanced view of the chemical compositions at a cross-link junction in a PEGDA hydrogel.[30] Reproduced in part from ref 30 with permission from Elsevier.

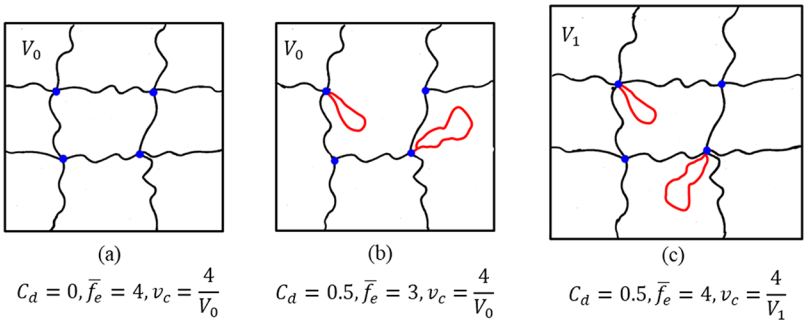

Figure 2. 2D schematic of (a) an ideal tetrafunctional network, (b) a nonideal hydrogel network with reduced effective functionality, and (c) a nonideal model with lower cross-link density (note that the volume is increased). Cross-link junctions are shown as blue dots, and loop defects are shown in red.

$$\bar{f}_e = \bar{f} - kC_d \tag{3}$$

where k is 2 for first-order loops because two chain ends are connected to a single junction and C_d is the average number of first-order loops per cross-link junction. Clearly, with the addition of first-order loops, the effective functionality is lower than the cross-link functionality. Note, additional defects such as dangling chains and unreacted "free" chains can be considered by expanding eq 3.

2.3. Construction of an Ideal Network Hydrogel. The ideal network model is commonly utilized in atomistic simulations of hydrogel behavior because of its well-defined structure.[36−38,45] It is employed initially in this study to provide a comparison with loop-containing models. To construct an ideal network model, six PEGDA chains are created with one end of each chain connected at a center point to form a cross-link junction and the other end extended in three perpendicular directions away from the junction, as illustrated in Figure 1. The cross-link junction is then replicated in three coordinate directions and connected with appropriate covalent bonds to form a cross-linked polymer network. Water molecules are added in small increments into the simulation cell during a MD simulation with temperature and pressure control (298 K and 1 atm) until the hydrogel model reaches 20 wt % PEGDA concentration.

2.4. Construction of Loop-Containing Hydrogels. Loop defects can be classified into different orders of connections depending on the number of cross-link junctions involved. The first-order loop, where two ends of a polymer chain connect at the same cross-link junction, has the most negative impact on the mechanical properties of hydrogels because it is fully inactive during deformation.[18] Therefore, this study uses first-order loops to understand the influence of defects on the high strain rate behavior of hydrogels.

Two approaches are proposed to introduce loop defects, shown schematically in 2D in Figure 2. In the ideal network (Figure 2a), the average number of defects per cross-link junction (C_d) is 0 since no defects exist. A cross-link density (ν_c) of $\frac{4}{V_0}$ is achieved by the presence of four junctions (blue dots) within the volume V_0. Furthermore, each cross-link junction has four active connections, which results in an effective functionality ($\bar{f}_e$) of 4. The first approach to introduce loop defects involves changes in effective functionality of the network, where active chains in the ideal network are replaced with first-order loops. For the 2D example in Figure 2b, the effective cross-link functionality decreases from 4 to 3 after loop replacement, while the cross-link density is unaltered. There are two loops and four cross-link junctions within the network. Therefore, a C_d of 0.5 is reached. The second approach allows changes in cross-link density, where the total number of active chains is maintained and two loops are added to the ideal network, as illustrated in 2D in Figure 2c. There are two loops out of four junctions, once again yielding a C_d of 0.5. Due to the addition of polymer chains, additional water molecules are added to maintain the same

https://dx.doi.org/10.1021/acs.jpcb.9b11378
J. Phys. Chem. B 2020, 124, 2029−2039

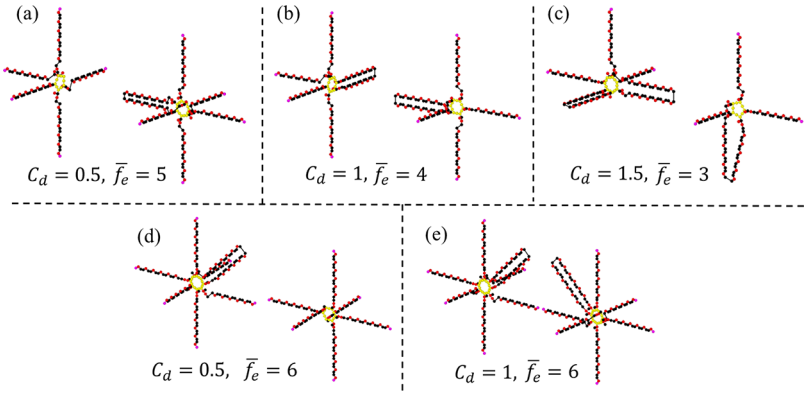

Figure 3. Junction template pairs for (a–c) loop-containing models with average effective functionalities from 5 to 3 but constant cross-link density; (d, e) models with different cross-link densties but fixed effective functionality.

PEGDA concentration of 20 wt %, which consequently increases the volume of the simulation cell and decreases the cross-link density as $\frac{4}{V_0} > \frac{4}{V_1}$. Thus, in this approach, the effective cross-link functionality is constant, but the cross-link density decreases. Both approaches are adopted in this study because they allow individual and systematic studies of the role of hydrogel network topological features in mechanical behavior.

The 2D templates shown in Figure 2 are not amenable to create 3D networks with the ability to vary effective cross-link functionality and cross-link density over a range of desired values. Therefore, templates are created with pairs of cross-link junctions, as shown in Figure 3. Similar to the ideal network model, each junction in the template consists of elastically active chains, which are connected at a center point and extend outward in three coordinate directions. Loops are then added to the template pair to reach a specific average number of defects per cross-link junction (C_d). Template pairs used to create hydrogel networks with different effective cross-link functionalities ranging from 5 to 3 are presented in Figures 3a–c, and template pairs used to create hydrogel networks with different cross-link densities are illustrated in Figures 3d–e.

Simulation cells with two different geometries are created for the two modes of deformation. Uniaxial tension is conducted with a cubic simulation box that contains 216 cross-link junctions with 6 junctions in each direction, while the simulation box for transient-state shear has 1536 junctions with 8 junctions in the x- and y-direction and 24 junctions in the z-direction. Templates of junction pairs are inserted into the simulation box considering periodic boundary conditions. Water molecules are added to reach 20 wt % PEGDA concentration. Equilibration is carried out in the isothermal–isobaric (NPT) ensemble at 298 K and 1 atm for 70 ps. Depending on the cross-link density, the length of equilibrated simulation box ranges from 155.8 to 168.6 Å for uniaxial tension, and from 205 to 226 Å in the x- and y-direction and 660 to 724 Å in the z-direction for transient-state shear. Three independent models with different random seeds are created, and the simulation results are presented as averages.

2.5. Measurement of Mesh Size. To calculate mesh size in MD simulation, a map of cross-link connectivity is recorded after the construction of each hydrogel network. Then, the center of mass position for each cross-link junction is tracked during each MD simulation. A mesh vector ($\vec{\xi}_a$) is calculated from the positions of two connected cross-link junctions, where the subscript a represents the initial x, y, or z orientation of the vector within the network. The mesh vector is then divided into three components based on the direction of the cross-link connection as $\vec{\xi}_{ab}$ where b is any one of three coordinate directions. The mesh size in each direction (ξ_a) is calculated as an average value of the magnitude of mesh vectors, and the average mesh size (ξ) is the mean value of mesh sizes in all directions. A schematic of the mesh vector during shear deformation is provided in Figure 4.

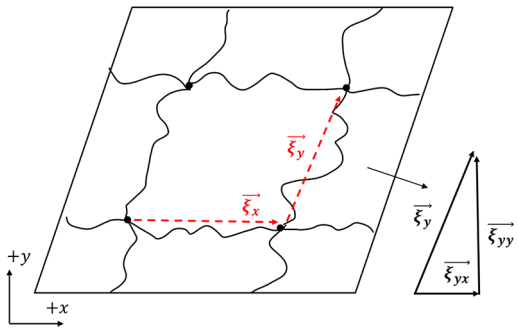

Figure 4. Schematic of the mesh vector $\vec{\xi}_a$ and mesh vector components $\vec{\xi}_{ab}$ in a hydrogel under shear deformation.

In addition to the measurement of mesh size, it is important to differentiate the stress state at each mesh size. The elongation of polymer chains consists of two stages.[37,46] The first stage involves conformational changes such as uncoiling, which leads to an entropy-driven low stress state. The second stage starts when the polymer chains are fully uncoiled, where bond stretching and deviation from equilibrium angle relationships occur upon further deformation, resulting in an enthalpy-related high stress state. Therefore, a theoretical value defined as the transition mesh size (ξ_t) is used to mark the transition point between these two stages. Using an average bond distance of 1.54 Å and an average angle of 110°, the transition mesh size is calculated as 49.19 Å for PEGDA13.[33]

3. SIMULATION RESULTS

3.1. Equilibrium Properties of Loop-Containing Hydrogels. The equilibrium properties of nonideal PEGDA hydrogels prepared with various effective functionalities and cross-link densities are provided in Tables 1 and 2,

https://dx.doi.org/10.1021/acs.jpcb.9b11378
J. Phys. Chem. B 2020, 124, 2029–2039

Table 1. Equilibrium Properties of 20 wt % PEGDA Hydrogels with Different Effective Cross-Link Functionalities

C_d	$\overline{f}$	$\overline{f}_e$	ν_c (mol/m^3)	ξ (Å)	ρ (g/cm^3)
0.0	6	6	94.64 ± 0.45	26.00 ± 0.04	1.046 ± 0.003
0.5	6	5	95.02 ± 0.28	27.17 ± 0.06	1.045 ± 0.004
1.0	6	4	95.07 ± 0.38	27.94 ± 0.05	1.047 ± 0.002
1.5	6	3	95.23 ± 0.81	28.27 ± 0.24	1.048 ± 0.008

Table 2. Equilibrium Properties of 20 wt % PEGDA Hydrogels with Various Cross-Link Densities

C_d	$\overline{f}$	$\overline{f}_e$	ν_c (mol/m^3)	ξ (Å)	ρ (g/cm^3)
0.0	6	6	94.64 ± 0.45	26.00 ± 0.04	1.046 ± 0.003
0.5	7	6	83.77 ± 0.11	27.06 ± 0.02	1.047 ± 0.001
1.0	8	6	74.87 ± 0.25	28.10 ± 0.03	1.047 ± 0.003

respectively. Ideal hydrogel models are included for comparison with defective hydrogels. Each calculation is averaged over three models with different random seeds for loop creation and temperature initialization. All hydrogel models exhibit similar densities of ∼1.047 g/cm^3 due to constant PEGDA concentration. In addition, hydrogels have equilibrium mesh sizes of ∼27 Å. For comparison, an equilibrium density of 1.021 g/cm^3 and an equilibrium mesh size of 30 Å are measured in experiments for PEGDA13 hydrogels with 20 wt % polymer concentration.[44,47] This represents the first validation of the proposed hydrogel model construction method. In Table 1, minimal difference is noted in cross-link density between models as designed. In Table 2, the cross-link density ν_c decreases by as much as ∼20% with constant effective functionality. These trends serve as the second validation of the loop-containing hydrogel models. The average mesh size in both approaches increases with the defect to cross-link junction ratio (C_d). This is explained by the balance between the thermodynamic force of swelling and retractive force of elastically active chains. For hydrogels with the same chain length, swelling behavior is inversely related to cross-link density while the retractive force is dependent on the number of active chains.[48] In hydrogels with different effective functionalities, the effect of fewer elastically active chains is compensated by the stretch of existing chains to maintain the same retractive force, while in models with various cross-link densities, lower cross-link densities from the insertion of loops lead to a larger swelling force. Therefore, active polymer chains are stretched to balance swelling behavior.

3.2. High Strain Rate Tensile Deformation of Hydrogels. Uniaxial tension is used as a simple loading condition to investigate the role of loop defects and to develop characterization methods for correlations between topology and mechanical response. Specifically, ideal and nonideal hydrogels are subjected to uniaxial tension using deformation−relaxation cycles. At the start of a cycle, a 3% strain is instantly imposed on the simulation domain in the x-direction and atom coordinates are rescaled to the new cell dimensions. Relaxation is then carried out with a Nosé−Hoover thermostat and barostat to control the temperature to 298.15 K and pressure to 1 atm in the y- and z-directions. The duration of relaxation determines the strain rate applied to the sample. A relaxation time of 30 ps is employed, resulting in a strain rate of 10^9/s. Stress is averaged over the last 5 ps of each relaxation. Note, bond breaking and other fracture mechanisms are not considered in this study due to the use of harmonic OPLS interatomic potentials. Thus, simulations are conducted until a predefined stress is reached, avoiding unrealistic stress states. Experimental results have shown that the ultimate stress in hydrogels at high strain rates (>10^3/s) is on the order of MPa.[5,22,28,49] Therefore, the deformation/relaxation cycles are performed until a stress level of 200 MPa is reached.

3.2.1. The Role of Effective Cross-Link Functionality. The stress−strain responses of PEGDA hydrogels with effective functionalities from 6 to 3 are shown in Figure 5a. All hydrogels exhibit similar stress−strain behaviors prior to ∼50% strain. For the ideal hydrogel ($\overline{f}_e = 6$), a rapid rise in stress is observed shortly after this point of demarcation. This rapid rise in stress is indicative of the two-stage of hydrogel deformation, as described in Section 2.5. For hydrogels with lower effective

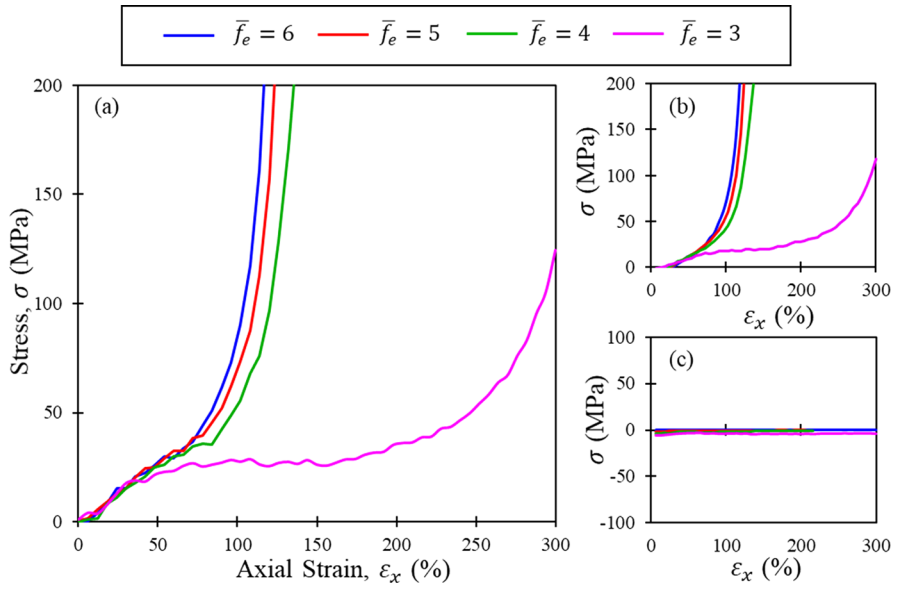

Figure 5. Stress−strain relationship of (a) hydrogels, (b) effective chains, and (c) loops with effective cross-link functionalities from 3 to 6.

https://dx.doi.org/10.1021/acs.jpcb.9b11378
J. Phys. Chem. B 2020, 124, 2029−2039

cross-link functionality ($\overline{f_e} < 6$), the rapid rise in stress is delayed until larger values of strain. This is particularly apparent in the hydrogel with $\overline{f_e} = 3$, where a plateau of stress is found between 50% and 200% strain. This delay indicates that the tensile deformation is not equally reflected on the elastically active chains of the hydrogel, which implies nonaffine movement of cross-link junctions[50] in defect-containing hydrogels at high strain (>50%) and in the high strain rate regime. The tensile stress−strain responses associated with active chains and loops are plotted in Figures 5b−c. Clearly, active chains are the dominant supporters of the total stress while the loops maintain a neutral stress state during the deformation. This observation agrees with prior theoretical and experimental studies[17,51] that loop defects are elastically inactive.

To correlate the tensile response with hydrogel topology in longitudinal and transverse directions, the evolutions of x- and y-direction mesh size ($\boldsymbol{\xi}_x$ and $\boldsymbol{\xi}_y$) for different $\overline{f_e}$ hydrogels are plotted in Figure 6. The predicted transition mesh size ($\boldsymbol{\xi}_t$) is also indicated to highlight the transition between deformation stages. Clearly, mesh sizes in the x- and y-directions have different behaviors due to the uniaxial loading condition. $\boldsymbol{\xi}_x$ in all hydrogels increase linearly at the same rate before ∼50% strain, suggesting an affine deformation stage. After 50% strain, the ideal hydrogel continues to exhibit the previous linear trend while lower $\overline{f_e}$ hydrogels show lower positive slopes in the mesh size versus strain relationship. This confirms nonaffine movement of the cross-link junctions in nonideal hydrogels, which corresponds to the stress reduction observed in Figure 5a. Meanwhile, the intercept with the transition mesh size, which reveals the transition from entropic- to enthalpic-driven deformation, increases at lower $\overline{f_e}$. This explains the delayed stress development in nonideal hydrogels. For validation, the intercept of $\boldsymbol{\xi}_x$ with the transition mesh size for the $\overline{f_e} = 3$ hydrogel is ∼200% strain, which matches the strain where a steep rise of stress begins, as shown in Figure 5a.

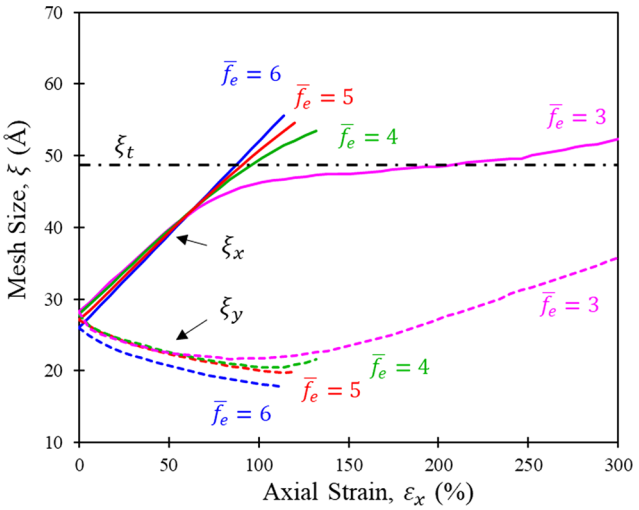

Figure 6. Evolution of mesh size in the x-direction (solid lines) and y-direction (dash lines) for hydrogels with effective cross-link functionalities from 6 to 3. The transition mesh size is indictaed as a horizontal dashed line.

In the y-direction, the mesh size of an ideal hydrogel exhibits a continuous decreasing trend because of the Poisson's effect. Note, nonlinearity is found in the trend of $\boldsymbol{\xi}_y$. This is likely due to the finite compressibility of polymer chains,[52,53] which leads to increased repulsive force between two approaching cross-link junctions in the transverse direction at higher strain and restricts additional reduction of $\boldsymbol{\xi}_y$. On the other hand, nonideal models show increased $\boldsymbol{\xi}_y$ after ∼100% strain. This is an indication that relative shear motion of cross-link junctions occurs due to realignment of PEGDA chains in the loading direction.

To quantify the degree of nonaffine cross-link junction motion, an active ratio is proposed

$$R_{\text{active}} = \frac{\overline{f_e}}{\overline{f_{ie}}} \frac{n_a |\overrightarrow{\xi_{aa}}|}{L_a} \tag{4}$$

where $\overline{f_{ie}}$ is the effective functionality of an ideal network ($\overline{f_{ie}} = 6$), n_a is the number of cross-link junctions in the a-direction, and L_a is the length of simulation box in the a-direction. Specifically, the active ratio quantifies the fraction of the simulation box that is occupied by elastically active chains. R_{active} in the x- and y-directions for different $\overline{f_e}$ hydrogels during uniaxial loading are presented in Figure 7a. The starting R_{active} at 0% strain is a direct representation of the $\frac{\overline{f_e}}{\overline{f_{ie}}}$ ratio, where the ideal hydrogel has a R_{active} of unity due to the absence of defects. In the x-direction, the ideal hydrogel exhibits a constant R_{active} during deformation, whereas decreasing trends of R_{active} with strain are observed for hydrogels with lower cross-link functionalities. This provides additional evidence that when the cross-link functionalities are less than ideal, the positions of cross-link junctions in the x-direction will rearrange during deformation to minimize the stretch of the active chains. In the y-direction, R_{active} is approximately constant for all hydrogels, suggesting that spatial rearrangement of junctions only occurs in the loading direction during uniaxial tension.

The difference between R_{active} from the initial state to the strained state (ΔR_{active}) in the x-direction represents the degree of spatial rearrangement of cross-link junctions. At 100% strain, hydrogels with $\overline{f_e} = 3$ have the highest ΔR_{active} of 8% while $\overline{f_e} = 6$ hydrogels have a ΔR_{active} of 0%. Clearly, a larger value of ΔR_{active} corresponds to a higher degree of junction rearrangement, which leads to the lower stress−strain responses seen in Figure 5a and lower positive slope in the $\boldsymbol{\xi}_x$ versus strain relationship in Figure 6. This statement is supported in Figure 7b−e by tracking the positions of cross-link junctions in ideal and $\overline{f_e} = 3$ hydrogels from virgin to deformed states. The reference postions for the cross-link junctions under affine translation are shown using a grid. In ideal hydrogels, cross-link junctions align with the grid throughout the uniaxial tensile deformation. On the contrary, cross-link junctions in $\overline{f_e} = 3$ hydrogels align with grid at 0% strain while clear rearrangement relative to the grid occurs at 114% strain.

3.2.2. The Role of Cross-Link Density. Uniaxial stress−strain responses for hydrogels with different cross-link densities are provided in Figure 8. Hydrogels with lower ν_c show earlier transitions from entropic to enthalpic deformation stages and

https://dx.doi.org/10.1021/acs.jpcb.9b11378
J. Phys. Chem. B 2020, 124, 2029−2039

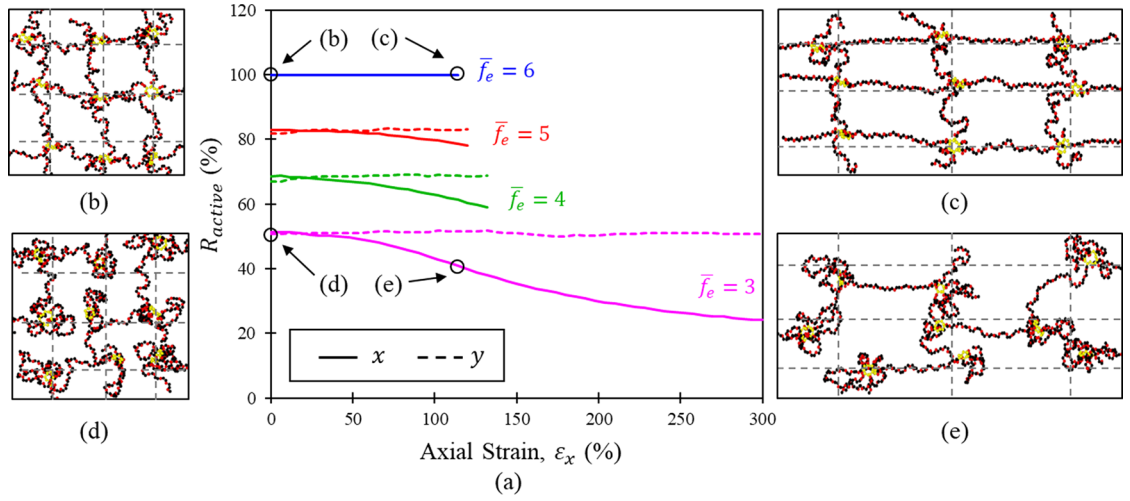

Figure 7. (a) x- and y-direction active ratios versus strain for hydrogels with effective functionalities from 6 to 3. Cross-linked structure of ideal hydrogels at (b) 0% strain and (c) 114% strain. Cross-linked structure of hydrogels with effective functionality of 3 at (d) 0% strain and (e) 114% strain. The grid provides the reference postions for cross-link junctions under affine uniaxial deformation.

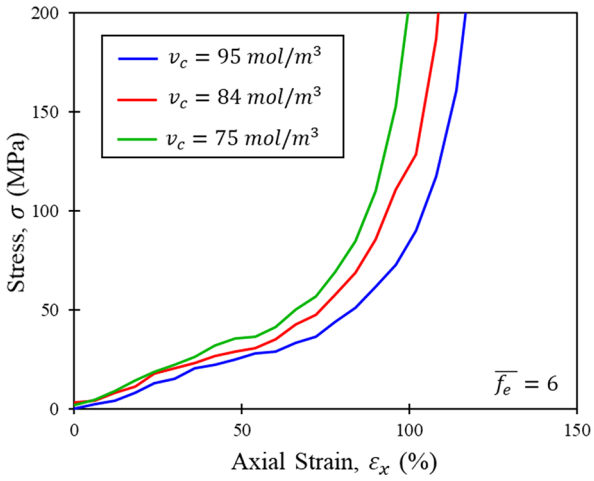

Figure 8. Stress−strain relationship of hydrogels with different cross-link densities.

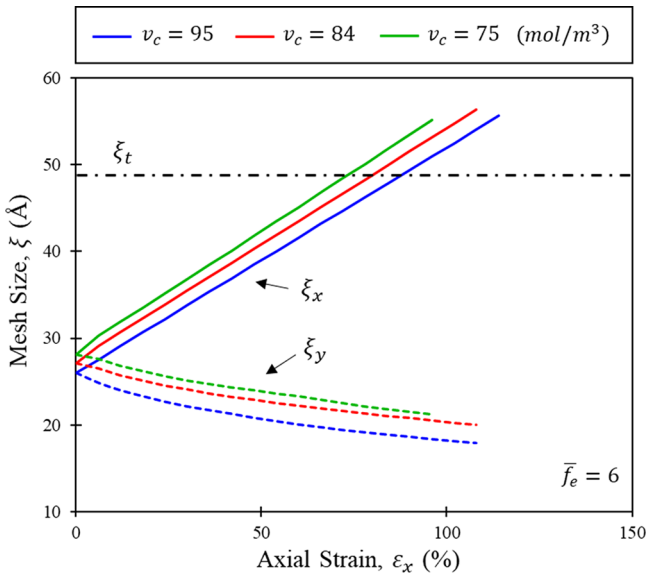

Figure 9. Evolution of mesh size in the x-direction (solid lines) and y-direction (dash lines) for hydrogels with different cross-link densities.

higher stress levels throughout the entire deformation. The mesh sizes in the x- and y-directions during uniaxial tension are shown in Figure 9. Lower v_c hydrogels exhibit a higher initial mesh size due to swelling. During deformation, $\boldsymbol{\xi}_x$ in all hydrogels increases at a constant rate with strain, indicating affine movement of the cross-link junction positions. Due to higher initial mesh size, less strain is required for lower v_c hydrogels to reach the transition mesh size, which corresponds to the earlier rise of stress in Figure 8. On the other hand, hydrogels with different v_c exhibit similar decreasing trends in $\boldsymbol{\xi}_y$. No increase in $\boldsymbol{\xi}_y$ is seen, contrary to that shown in Figure 6 for hydrogels with different effective functionalities. This behavior confirms that no spatial rearrangement of cross-link junctions occurs.

In summary, the influence of first-order loop defects on the behavior of hydrogels under high strain rate uniaxial tensile deformation depends on the network topology. Hydrogels with lower effective functionalities exhibit nonaffine translation of the cross-link junctions during uniaxial tension, which results in lower stress states with significant spatial rearrangement of the junction positions. In contrast, hydrogels with different cross-link densities but a constant effective functionality show no cross-link junction rearrangement during the deformation process. In this case, lower cross-link densities increase the initial mesh size and promote a higher stress state.

3.3. Transient-State Shear Deformation. The transient-state shear deformation of hydrogels is conducted using the boundary-driven method.[30] Lennard-Jones (LJ) atoms arranged in a face-centered cubic (fcc) crystal structure are placed at the left and right surface of the simulation box as the boundary walls, with (111) surface facing the hydrogel. The LJ size parameter is 3.5 Å, and energy parameter is 1.867 785 kcal/mol.[54] The wall−hydrogel interaction is calculated using Lorentz−Berthelot rules. Each wall has a thickness of 18 Å and is treated as a rigid body. MD simulations with the canonical ensemble (NVT) are performed for 300 ps, where the stress between the walls and the hydrogel is relaxed. Temperature is set at 298 K using a Nosé−Hoover thermostat. Dynamic shear deformation is carried out with a constant acceleration applied to the left wall of the model in the positive x-direction, as

https://dx.doi.org/10.1021/acs.jpcb.9b11378
J. Phys. Chem. B 2020, 124, 2029−2039

shown in Figure 10. The momentum diffusion length is calculated as

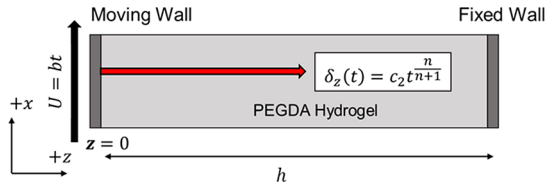

Figure 10. Schematic of transient-state shear simulation.[33] The black arrows represent input velocity and its direction; the red arrows represent the momentum diffusion lenth and its direction. Reproduced from ref 33 with permission from the American Chemical Society.

$$\delta_z(t) = \frac{2}{x_d(t, 0)} \int_0^h x_d(t, z)\mathrm{d}z \tag{5}$$

where δ_z is the momentum diffusion length, h is the length of hydrogel model in the z-direction, and x_d is the displacement in the x-direction. A self-similar solution is applied to capture relationship between the momentum diffusion length and diffusion[32]

$$\delta_z(t) = c_2 t^{n/n+1} \tag{6}$$

where c_2 is a material constant and n denotes the shear-thickening exponent. In eq 6, the shear-thickening exponent n is a dimensionless (time independent) variable that describes the level of shear-thickening behavior in hydrogels. This exponent is used as a metric to study the influence of loop defects on the high strain rate shear behavior of hydrogels. Additional details of the simulation configuration and constitutive modeling can be found in authors' previous studies.[32,33]

3.3.1. The Role of Effective Cross-Link Functionality. The computed shear-thickening exponents for hydrogels with $\overline{f_e}$ from 6 to 3 are shown in Table 3. An experimental result for 20 wt % PEGDA hydrogels is included for comparison.[33] The upper and lower limits of the shear-thickening exponent are provided in the brackets. The experimental data shows a shear-thickening value between the simulation results of hydrogels with $\overline{f_e}$ of 6 and 5, which implies a defect per cross-link junction ratio (C_d) between 0 and 0.5. This range agrees with observations made in prior experimental studies on PEGDA hydrogels,[55] which again provides validation for the nonideal hydrogel model construction method. Furthermore, lower shear-thickening exponents are found in lower effective functionality hydrogels. This is expected as fewer active chains are involved in deformation and more intense junction spatial rearrangements occur, analogous to the case of uniaxial tension.

The evolution of mesh size is used to study the correlation between shear-thickening response and network topology. Figure 11 presents the average z-direction mesh size within the momentum diffusion region. Second-order polynomial fits with a least-squares approach are applied to describe the mesh size versus time relationship. The ideal hydrogel has the smallest initial $\langle \xi_z \rangle_m$ but demonstrates the fastest increase during shear deformation. In contrast, hydrogels with $\overline{f_e} = 3$ have the largest initial $\langle \xi_z \rangle_m$ and the lowest increasing rate. The average mesh size is below the transition mesh size; however, individual PEGDA chains within the momentum diffusion region do exceed the transition mesh size. Thus, a distribution is achieved where the highest mesh size is computed near the shear boundary and lowest mesh size is computed at the momentum diffusion front.[33] A slower increase in $\langle \xi_z \rangle_m$ implies that fewer chains have exceeded the transition mesh size at a specific point in time. This explains the lower shear-thickening exponent observed in hydrogels with lower $\overline{f_e}$.

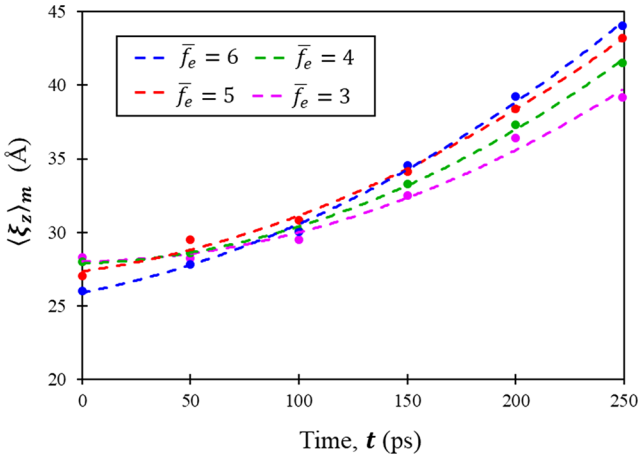

Figure 11. Evolution of average mesh size within the momentum diffusion region along the z-direction for hydrogels with effective cross-link functionalities from 6 to 3 during transient-state shear deformation.

To elucidate the mechanism responsible for the behavior in Figure 11, the x and z components of $\langle \xi_z \rangle_m$ are calculated and shown in Figures 12a–b. In Figure 12a, all hydrogels have nonzero initial $\langle \xi_{zx} \rangle_m$ since the positions of cross-link junctions move during the thermal equilibration procedure. After 50 ps, slower increasing trends are computed for lower $\overline{f_e}$ hydrogels. In Figure 12b, the evolution of $\langle \xi_{zz} \rangle_m$ is plotted. $\langle \xi_{zz} \rangle_m$ decreases in all nonideal models while it remains nearly constant in the ideal hydrogel. The above results demonstrate the spatial rearrangement of cross-link junctions in both x- and z-directions during the transient-state shear deformation.

R_{active} in three coordinate directions as a function of time is plotted in Figure 13 to quantify the direction and magnitude of junction rearrangements within the hydrogel. In models with reduced $\overline{f_e}$, R_{active} decreases in all three directions, with R_{active} in the z-direction having the largest decrease. This trend supports the observation that three-dimensional spatial rearrangements of cross-link junctions occur during shear deformation and the momentum diffusion direction demon-

Table 3. Computed Average Shear-Thickening Exponents of 20 wt % PEGDA Hydrogels with Different Effective Functionalities

$\overline{f_e}$	6	5	4	3	Experiment[33]
n	4.79 (3.45–7.69)	3.37 (2.75–4.22)	2.15 (1.91–2.44)	2.06 (1.80–2.39)	3.65 (2.55–5.76)

https://dx.doi.org/10.1021/acs.jpcb.9b11378
J. Phys. Chem. B 2020, 124, 2029–2039

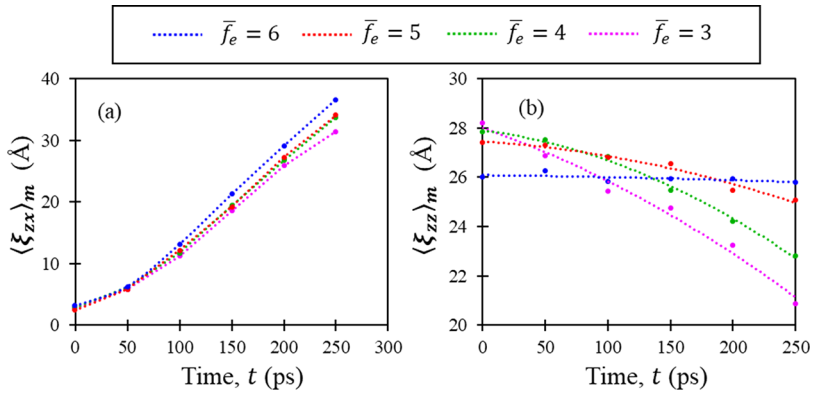

Figure 12. Evolution of (a) x component and (b) z component of the average z-direction mesh size for hydrogels with effective cross-link functionalities from 3 to 6.

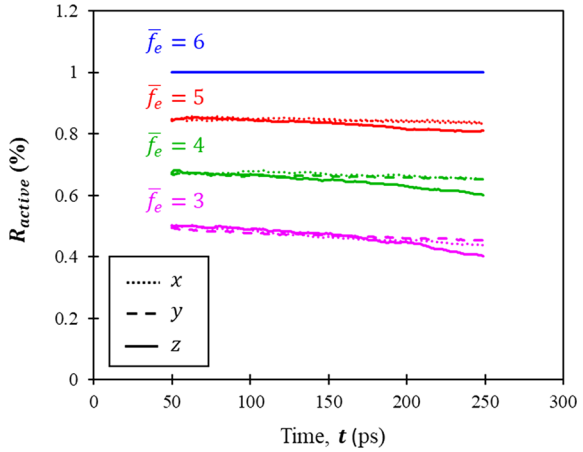

Figure 13. Active ratio versus strain in three coordinate directions for hydrogels with effective cross-link functionalities from 3 to 6.

strates the highest level of rearrangement. In addition, different magnitudes of ΔR_{active} are observed depending on $\bar{f}_e$, where $\bar{f}_e = 3$ hydrogels have the lowest ΔR_{active} of 12% at a time of 250 ps, suggesting that the magnitude of spatial rearrangement increases for hydrogels with lower $\bar{f}_e$. This conclusion agrees with the results of uniaxial tension simulations, where greater spatial rearrangements of cross-link junctions are observed in lower $\bar{f}_e$ hydrogels.

3.3.2. The Role of Cross-Link Density. Shear-thickening exponents for hydrogels as a function of cross-link density are provided in Table 4. The presence of loops in the ideal network, which provides a decrease in cross-link density, has negligible influence on shear-thickening behavior.

The evolution of the average z-direction mesh size within the momentum diffusion region is plotted in Figure 14a. Hydrogels with the lowest ν_c have the highest initial $\langle \xi_z \rangle_m$. However, as opposed to the results in Figure 11, the rate of mesh size increase is very similar for each model. As the evolution of mesh size determines the stress state during shear deformation, this suggests similar shear-thickening behaviors, which concurs with the data in Table 4. The x and z components of the average z-direction mesh size are computed and displayed in Figure 14b–c to explain this observation. The reduction in cross-link density does not alter the behavior of $\langle \xi_{zx} \rangle_m$ and $\langle \xi_{zz} \rangle_m$, implying that shear deformation is equally reflected in the active chains regardless of the density of inserted first-order loops. This agrees with the observation in uniaxial tension deformation that decreases in cross-link density do not promote nonaffine motion of the cross-link junction positions.

Table 4. Computed Average Shear-Thickening Exponents of 20 wt % PEGDA Hydrogels with Different Cross-Link Densities

ν_c (mol/m^3)	95	84	75
n	4.79 (3.45–7.69)	4.42 (3.40–6.05)	4.92 (4.15–5.96)

4. SUMMARY

Nonideal hydrogel models are created via two approaches to study the influence of first-order loop defects on the high strain rate behavior of hydrogels. The first approach allows different effective functionalities with constant cross-link density within the hydrogel network, by replacing elastically active chains with first-order loop defects. The second approach alters the cross-link densities while keeping the cross-link effective functionality constant, by adding additional loops into an existing cross-linked network. The nonideal hydrogel construction method is unique and provides a systematic way to study the individual role of different topological variables that describe the cross-linked network in a hydrogel.

High strain rate uniaxial tension and transient-state shear MD simulations are performed. Simulations prove that loop defects are elastically inactive; however, the topological changes caused by the introduction of loop defects can influence the high strain rate behavior of hydrogels. Lower stresses and reduced shear-thickening behavior are found in hydrogels with lower effective cross-link functionalities. This is caused by nonaffine movements of the cross-link junctions within the nonideal network that alleviate the stretch of elastically active chains. The extent of nonaffine cross-link junction movements is quantified by computing the change of active ratio in the deforming direction. In hydrogels with lower cross-link densities but with a constant effective functionality, swelling causes increases in the initial mesh size. Thus, under tensile deformation, the strain necessary to reach the transition mesh size between entropic and enthalpic deformation regimes decreases, and an earlier rise in stress is observed. However, because the topology of the hydrogel network does not spatially rearrange during deformation and the changes in cross-link density are not sufficiently large, a similar shear-

https://dx.doi.org/10.1021/acs.jpcb.9b11378
J. Phys. Chem. B 2020, 124, 2029–2039

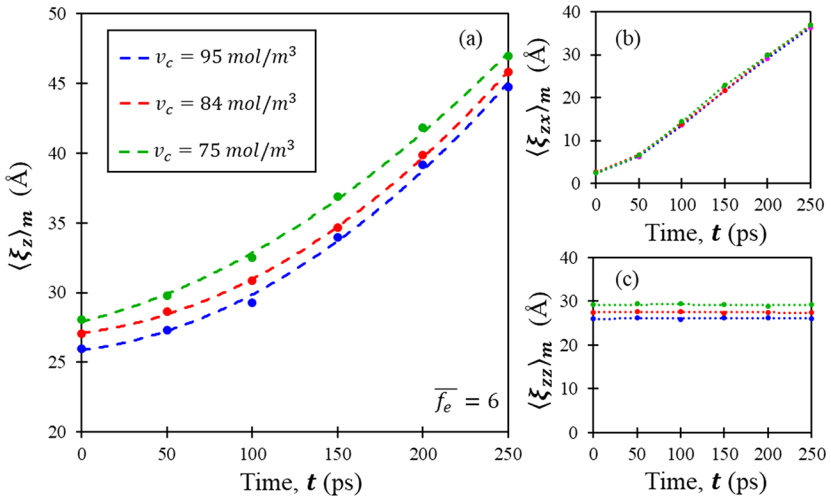

Figure 14. Evolution of (a) average mesh size in z-direction and its (b) x component and (c) z component within the momentum diffsion region for hydrogels with various cross-link densities during transient-state shear deformation.

thickening behavior is computed. Combined, reductions in effective cross-link functionality have a greater impact on the mechanical behavior of hydrogels than reductions in cross-link density.

The findings of this work provide insights that will assist defect aware constitutive modeling of tissue surrogates and help in the design of hydrogels with customized responses by controlling the type and density of defects.

AUTHOR INFORMATION

Corresponding Author

Douglas E. Spearot − *Department of Mechanical & Aerospace Engineering, University of Florida, Gainesville, Florida 433611, United States;* orcid.org/0000-0003-1875-6036; Phone: 352-392-6747; Email: dspearot@ufl.edu

Authors

Ke Luo − *Department of Materials Science & Engineering, University of Florida, Gainesville, Florida 433611, United States*

Charity Wangari − *Department of Mechanical & Aerospace Engineering, University of Florida, Gainesville, Florida 433611, United States*

Ghatu Subhash − *Department of Mechanical & Aerospace Engineering, University of Florida, Gainesville, Florida 433611, United States;* orcid.org/0000-0002-5996-0909

Complete contact information is available at: https://pubs.acs.org/10.1021/acs.jpcb.9b11378

Notes

The authors declare no competing financial interest.

ACKNOWLEDGMENTS

This work was supported by the National Science Foundation under grants CMMI-1634188 and CMMI-1762791. C.W. was supported by the National Science Foundation via the REU Site: Engineering for Healthcare EEC-1757128. The authors acknowledge the University of Florida Research Computing for providing computational resources.

REFERENCES

(1) Okay, O. *Hydrogel Sensors and Actuators*; Gerlach, G., Arndt, K.-F., Eds.; Springer Series on Chemical Sensors and Biosensors; Springer Berlin Heidelberg: Berlin, Heidelberg, 2010; Vol. *6*.

(2) El-Sherbiny, I. M.; Yacoub, M. H. Hydrogel Scaffolds for Tissue Engineering: Progress and Challenges. *Glob. Cardiol. Sci. Pract.* **2013**, *2013*, 316−342.

(3) Ahmed, E. M. Hydrogel: Preparation, Characterization, and Applications: A Review. *J. Adv. Res.* **2015**, *6*, 105−121.

(4) Drury, J. L.; Mooney, D. J. Hydrogels for Tissue Engineering: Scaffold Design Variables and Applications. *Biomaterials* **2003**, *24*, 4337−4351.

(5) Naarayan, S. S.; Subhash, G. Wave Propagation in Ballistic Gelatine. *J. Mech. Behav. Biomed. Mater.* **2017**, *68*, 32−41.

(6) Flory, P. J.; Rehner, J. Statistical Mechanics of Cross-Linked Polymer Networks I. Rubberlike Elasticity. *J. Chem. Phys.* **1943**, *11*, 512−520.

(7) Flory, P. J. Network Topology and the Theory of Rubber Elasticity. *Br. Polym. J.* **1985**, *17*, 96−102.

(8) Flory, P. J. Theory of Elasticity of Polymer Networks. The Effect of Local Constraints on Junctions. *J. Chem. Phys.* **1977**, *66*, 5720−5729.

(9) Zhou, H.; Schön, E.-M.; Wang, M.; Glassman, M. J.; Liu, J.; Zhong, M.; Díaz Díaz, D.; Olsen, B. D.; Johnson, J. A. Crossover Experiments Applied to Network Formation Reactions: Improved Strategies for Counting Elastically Inactive Molecular Defects in PEG Gels and Hyperbranched Polymers. *J. Am. Chem. Soc.* **2014**, *136*, 9464−9470.

(10) Solomon, D. H.; Cacioli, P.; Moad, G. Structural Defects in Polymers - Their Identification and Significance. *Pure Appl. Chem.* **1985**, *57*, 985−992.

(11) Gu, Y.; Zhao, J.; Johnson, J. A. A (Macro)Molecular-Level Understanding of Polymer Network Topology. *Trends Chem.* **2019**, *1*, 318−334.

(12) Wang, R.; Alexander-Katz, A.; Johnson, J. A.; Olsen, B. D. Universal Cyclic Topology in Polymer Networks. *Phys. Rev. Lett.* **2016**, *116*, 188302.

(13) Kawamoto, K.; Zhong, M.; Wang, R.; Olsen, B. D.; Johnson, J. A. Loops versus Branch Functionality in Model Click Hydrogels. *Macromolecules* **2015**, *48*, 8980−8988.

(14) Wang, R.; Johnson, J. A.; Olsen, B. D. Odd-Even Effect of Junction Functionality on the Topology and Elasticity of Polymer Networks. *Macromolecules* **2017**, *50*, 2556−2564.

(15) Lang, M. Elasticity of Phantom Model Networks with Cyclic Defects. *ACS Macro Lett.* **2018**, *7*, 536−539.

(16) Chan, D.; Ding, Y.; Dauskardt, R. H.; Appel, E. A. Engineering the Mechanical Properties of Polymer Networks with Precise Doping of Primary Defects. *ACS Appl. Mater. Interfaces* **2017**, *9*, 42217−42224.
(17) Akagi, Y.; Matsunaga, T.; Shibayama, M.; Chung, U.-i.; Sakai, T. Evaluation of Topological Defects in Tetra-PEG Gels. *Macromolecules* **2010**, *43*, 488−493.
(18) Zhong, M.; Wang, R.; Kawamoto, K.; Olsen, B. D.; Johnson, J. A. Quantifying the Impact of Molecular Defects on Polymer Network Elasticity. *Science* **2016**, *353*, 1264−1268.
(19) Wang, J.; Lin, T. S.; Gu, Y.; Wang, R.; Olsen, B. D.; Johnson, J. A. Counting Secondary Loops Is Required for Accurate Prediction of End-Linked Polymer Network Elasticity. *ACS Macro Lett.* **2018**, *7*, 244−249.
(20) Anseth, K. S.; Bowman, C. N.; Brannon-Peppas, L. Mechanical Properties of Hydrogels and Their Experimental Determination. *Biomaterials* **1996**, *17*, 1647−1657.
(21) Wang, Y.; Wang, S.; Xu, C.; Xuan, S.; Jiang, W.; Gong, X. Dynamic Behavior of Magnetically Responsive Shear-Stiffening Gel under High Strain Rate. *Compos. Sci. Technol.* **2016**, *127*, 169−176.
(22) Richler, D.; Rittel, D. On the Testing of the Dynamic Mechanical Properties of Soft Gelatins. *Exp. Mech.* **2014**, *54*, 805−815.
(23) Doman, D. A.; Cronin, D. S.; Salisbury, C. P. Characterization of Polyurethane Rubber at High Deformation Rates. *Exp. Mech.* **2006**, *46*, 367−376.
(24) Appleby-Thomas, G. J.; Hazell, P. J.; Sheldon, R. P.; Stennett, C.; Hameed, A.; Wilgeroth, J. M. The High Strain-Rate Behaviour of Selected Tissue Analogues. *J. Mech. Behav. Biomed. Mater.* **2014**, *33*, 124−135.
(25) Appleby-Thomas, G. J.; Hazell, P. J.; Wilgeroth, J. M.; Shepherd, C. J.; Wood, D. C.; Roberts, A. On the Dynamic Behavior of Three Readily Available Soft Tissue Simulants. *J. Appl. Phys.* **2011**, *109*, 084701.
(26) Upadhyay, K.; Bhattacharyya, A.; Subhash, G.; Spearot, D. E. Quasi-Static and High Strain Rate Simple Shear Characterization of Soft Polymers. *Exp. Mech.* **2019**, *59*, 733−747.
(27) Liu, Q.; Subhash, G. Characterization of Viscoelastic Properties of Polymer Bar Using Iterative Deconvolution in the Time Domain. *Mech. Mater.* **2006**, *38*, 1105−1117.
(28) Kwon, J.; Subhash, G. Compressive Strain Rate Sensitivity of Ballistic Gelatin. *J. Biomech.* **2010**, *43*, 420−425.
(29) Upadhyay, K.; Subhash, G.; Spearot, D. Visco-Hyperelastic Constitutive Modeling of Strain Rate Sensitive Soft Materials. *J. Mech. Phys. Solids* **2020**, *135*, 103777.
(30) Luo, K.; Yudewitz, N.; Subhash, G.; Spearot, D. E. *Effect of Water Concentration on the Shock Response of Polyethylene Glycol Diacrylate (PEGDA) Hydrogels: A Molecular Dynamics Study* **2019**, *90*, 30−39.
(31) Subhash, G.; Kwon, J.; Mei, R.; Moore, D. F. Non-Newtonian Behavior of Ballistic Gelatin at High Shear Rates. *Exp. Mech.* **2012**, *52*, 551−560.
(32) Kwon, J.; Subhash, G.; Mei, R.; Heger, I. An Optical Technique for Determination of Rheological Properties of Gelatin. *J. Rheol. (Melville, NY, U. S.)* **2011**, *55*, 951−964.
(33) Luo, K.; Upadhyay, K.; Subhash, G.; Spearot, D. E. Transient-State Rheological Behavior of Poly(Ethylene Glycol) Diacrylate Hydrogels at High Shear Strain Rates. *Macromolecules* **2019**, *52*, 5860.
(34) Chiessi, E.; Cavalieri, F.; Paradossi, G. *J. Phys. Chem. B* **2007**, *111*, 2820−2827.
(35) Oelmeier, S. A.; Dismer, F.; Hubbuch, J. Molecular Dynamics Simulations on Aqueous Two-Phase Systems - Single PEG-Molecules in Solution. *BMC Biophys.* **2012**, *5*, 14.
(36) Lee, S. G.; Brunello, G. F.; Jang, S. S.; Bucknall, D. G. Molecular Dynamics Simulation Study of P (VP-Co-HEMA) Hydrogels: Effect of Water Content on Equilibrium Structures and Mechanical Properties. *Biomaterials* **2009**, *30*, 6130−6141.
(37) Jang, S. S.; Goddard, W. A.; Kalani, M. Y. S. Mechanical and Transport Properties of the Poly(Ethylene Oxide)−Poly(Acrylic Acid) Double Network Hydrogel from Molecular Dynamic Simulations. *J. Phys. Chem. B* **2007**, *111*, 1729−1737.
(38) Sun, D.; Zhou, J. Effect of Water Content on Microstructures and Oxygen Permeation in PSiMA−IPN−PMPC Hydrogel: A Molecular Simulation Study. *Chem. Eng. Sci.* **2012**, *78*, 236−245.
(39) Torres-Knoop, A.; Kryven, I.; Schamboeck, V.; Iedema, P. D. Modeling the Free-Radical Polymerization of Hexanediol Diacrylate (HDDA): A Molecular Dynamics and Graph Theory Approach. *Soft Matter* **2018**, *14*, 3404−3414.
(40) Rukmani, S. J.; Lin, P.; Andrew, J. S.; Colina, C. M. Molecular Modeling of Complex Cross-Linked Networks of PEGDA Nanogels. *J. Phys. Chem. B* **2019**, *123*, 4129−4138.
(41) Rizzo, R. C.; Jorgensen, W. L. OPLS All-Atom Model for Amines: Resolution of the Amine Hydration Problem. *J. Am. Chem. Soc.* **1999**, *121*, 4827−4836.
(42) Price, D. J.; Brooks, C. L. A Modified TIP3P Water Potential for Simulation with Ewald Summation A Modified TIP3P Water Potential for Simulation with Ewald Summation. *J. Chem. Phys.* **2004**, *121*, 10096.
(43) Plimpton, S. Fast Parallel Algorithms for Short-Range Molecular Dynamics. *J. Comput. Phys.* **1995**, *117*, 1−19.
(44) Ju, H.; McCloskey, B. D.; Sagle, A. C.; Kusuma, V. A.; Freeman, B. D. Preparation and Characterization of Crosslinked Poly(Ethylene Glycol) Diacrylate Hydrogels as Fouling-Resistant Membrane Coating Materials. *J. Membr. Sci.* **2009**, *330*, 180−188.
(45) Lee, H.; Venable, R. M.; MacKerell, A. D.; Pastor, R. W. Molecular Dynamics Studies of Polyethylene Oxide and Polyethylene Glycol: Hydrodynamic Radius and Shape Anisotropy. *Biophys. J.* **2008**, *95*, 1590−1599.
(46) Heymann, B.; Grubmüller, H. Elastic Properties of Poly-(Ethylene-Glycol) Studied by Molecular Dynamics Stretching Simulations. *Chem. Phys. Lett.* **1999**, *307*, 425−432.
(47) Witte, R. P.; Blake, A. J.; Palmer, C.; Kao, W. J. Analysis of Poly(Ethylene Glycol)-Diacrylate Macromer Polymerization within a Multicomponent Semi-Interpenetrating Polymer Network System. *J. Biomed. Mater. Res.* **2004**, *71A*, 508−518.
(48) Allin, S. B. Introduction to Physical Polymer Science, 3rd Edition. *J. Chem. Educ.* **2001**, *78*, 1469.
(49) Cronin, D. S.; Falzon, C. Dynamic Characterization and Simulation of Ballistic Gelatin. In *SEM Conference & Exposition on Experimental & Applied Mechanics*, Albuquerque, NM, 2009.
(50) Wen, Q.; Basu, A.; Janmey, P. A.; Yodh, A. G. Non-Affine Deformations in Polymer Hydrogels. *Soft Matter* **2012**, *8*, 8039.
(51) Zhou, H.; Woo, J.; Cok, A. M.; Wang, M.; Olsen, B. D.; Johnson, J. A. Counting Primary Loops in Polymer Gels. *Proc. Natl. Acad. Sci. U. S. A.* **2012**, *109*, 19119−19124.
(52) Leermakers, F. A. M.; Skvortsov, A. M.; Klushin, L. I. Negative Compressibility for a Polymer Chain Squeezed between Two Pistons Going through the Escape Transition. *J. Stat. Mech.: Theory Exp.* **2004**, *2004*, P10001.
(53) Brandt, W. Calculation of Compressibilities of High Polymers from the Energy of Interaction between Chain Groups. *J. Chem. Phys.* **1957**, *26*, 262−270.
(54) Leng, Y.; Cummings, P. T. Fluidity of Hydration Layers Nanoconfined between Mica Surfaces. *Phys. Rev. Lett.* **2005**, *94*, 026101.
(55) Zhou, H.; Woo, J.; Cok, A. M.; Wang, M.; Olsen, B. D.; Johnson, J. A. Counting Primary Loops in Polymer Gels. *Proc. Natl. Acad. Sci. U. S. A.* **2012**, *109*, 19119−19124.

https://dx.doi.org/10.1021/acs.jpcb.9b11378
J. Phys. Chem. B 2020, 124, 2029−2039